High-resolution offshore wind resource assessment at turbine hub height with Sentinel-1 SAR data and machine learning

Louis de Montera[1], Henrick Berger[1], Romain Husson[1], Pascal Appelghem[2], Laurent Guerlou[1], Mauricio Fragoso[1]

[1]CLS Collecte Localisation Satellites, Ramonville-Saint-Agne, France
[2]Atmosky, Talence, France

Correspondence to: Romain Husson (rhusson@groupcls.com)

Abstract. This paper presents a method for estimating the offshore extractible wind power at hub height using Sentinel-1 Synthetic Aperture Radar (SAR) data and machine learning. The method is tested in two areas off the Dutch coast where measurements from Doppler wind Lidars installed at the sea surface are available and can be used as a reference. A first machine learning algorithm improves the accuracy of SAR sea surface wind speeds by using geometrical characteristics of the sensor and metadata. This algorithm is trained with wind data measured by a large network of metocean buoys at 4 m above sea level. After correction, the bias of SAR wind speed at 4 m against buoys is 0.02 m s^{-1} and the standard deviation of its error is 0.74 m s^{-1}. Then, corrected surface wind speeds are extrapolated to hub height with a second machine learning algorithm, which uses meteorological parameters extracted from a high-resolution numerical model. This algorithm is trained with Lidar vertical wind profiles and can extrapolate sea surface wind speeds to various altitudes up to 200 m. Once wind speeds at hub height are obtained, the Weibull parameters of their distribution are estimated, taking into account the satellites irregular temporal sampling. Finally, we assume the presence of a 10 MW turbine and obtain the extractible wind power with a 1 km spatial resolution by multiplying the Weibull distribution point-by-point by its power curve. The accuracy of the extractible power against Lidars is ±3%. Wind power maps at hub height are presented and compared with the outputs of the numerical model. The maps based on SAR data have a much higher level of detail, especially regarding the coastal wind gradient. We conclude that SAR data combined with machine learning can improve the estimation of the extractible power at hub height and provide useful insights for optimizing siting and risk management. The algorithms presented in this study are independent and can also be used in a more general context to correct SAR surface winds, extrapolate surface winds to higher altitudes, or produce instantaneous SAR wind fields at hub height.

1 Introduction

Estimating the extractible offshore wind power at turbine hub height is a challenging problem due to the difficulty in measuring the wind profile in the boundary layer over sea. Currently, this quantity is estimated by using numerical models and/or Doppler wind Lidars installed at the sea surface pointing upwards (see, e.g., NREL, 2020). Lidars provide the complete wind profile at one location with a high temporal sampling, but are very expensive to operate. Therefore, only one or two are typically used to sound large areas. Conversely, numerical models provide outputs over the entire area of interest, but they are not capable of resolving small-scale phenomena due to their physics and resolution. As a result, their errors are not precisely known and may vary in time and space, which is particularly problematic in coastal areas where processes are more complex and involve smaller scales. Due to these limitations, considerable uncertainty remains about actual offshore wind resources, which can affect wind farm project planning and management.

The need for improving wind speed assessment, and thus estimating more precisely wind power availability throughout wind farms' life cycle, has led to a growing interest in using satellite data (see, e.g., Hasager et al., 2015). Contrary to ground-based Lidars, spaceborne sensors have the advantage of sounding large areas. However, they also have limitations: their revisit period is typically long (a couple of days for Sentinel-1 in Europe) and they use an indirect measurement based on the sea state backscatter. Therefore, their measurements are impacted by several sources of potential error (low temporal sampling, sensor geometry, currents, algae, bright targets like ships, rain cells, bathymetry, turbulence, etc.). Moreover, the extrapolation of their measurements from sea surface to hub height is not an easy task due to the variety of meteorological conditions that may impact the wind speed extrapolation ratio.

Several studies attempted to assess offshore wind power potential with spaceborne scatterometers, such as ERS-1, ERS-2, NSCAT, QuickSCAT, and ASCAT (Sánchez et al., 2007; Pimenta et al., 2008; Karagali et al., 2014; Bentamy and Croize-Fillon, 2014; Remmers et al., 2019). However, the resolution of these instruments is at best 12.5 km^2, which is not adapted to coastal areas due to land contamination. Synthetic Aperture Radar (SAR) satellites are an interesting alternative because SAR wind products have a much finer resolution of 1 km. The potential of SAR data has already been assessed by numerous studies (Hasager et al., 2002; Hasager et al., 2005; Hasager et al., 2006; Christiansen et al., 2006; Hasager et al., 2011; Hasager et al., 2014; Chang et al., 2014; Chang et al., 2015; Hasager et al., 2020). However, validating SAR measurements with in-situ data has been limited (Ahsbahs et al., 2017; Badger et al., 2019; de Montera et al., 2020; Ahsbahs et al., 2020) and these studies concluded that important biases remained (the term 'in-situ' includes here profiling Lidars, although they use remote sensing). One reason is that SAR surface winds are obtained by inverting the backscatter with Geophysical Model Functions (GMFs) that were originally designed for scatterometers, although differences with the SAR backscatter may occur due to different resolutions and the lack of inter-calibration between these two technologies. Another reason is that GMFs were designed empirically using the European Centre for Medium-Range Weather Forecasts (ECMWF) numerical model as a reference, which may not be accurate in coastal areas (in-situ data were used only for validation and a posteriori bias correction, see Stoffelen et al., 2017, and references therein). In addition, GMFs may not fully capture the

complex relation between the sea state and wind speed, in particular because they assume a neutral atmosphere. Therefore, it is necessary to improve the accuracy of SAR wind speeds obtained with GMFs. This is particularly important since wind power is related to the cube of wind speed, and therefore very sensitive to estimation errors.

Regarding the extrapolation of surface wind speeds to higher altitudes, the statistical theory of turbulence provides theoretical wind profiles (see, e.g., Grachev and Fairall, 1996). However, the problem has not been satisfactorily solved and becomes increasingly critical as the typical height of wind turbines increases. Empirical evidence from offshore meteorological masts suggests that a simple power law could be sufficient to model the wind profile (Hsu et al., 1994). Nevertheless, above a few tens of meters, the power law model is questionable (see, e.g., Tieo et al., 2020). This limitation has led some authors to use numerical models outputs to improve the extrapolation to higher altitudes (Badger et al., 2016). The advantage of numerical models is that they provide information about atmospheric stability through parameters like surface temperature and surface heat flux. In Badger et al. (2016), these surface parameters were averaged and combined with the similarity theory of Monin-Obukhov to extrapolate wind Weibull parameters. However, to our knowledge, this method was validated with only one meteorological mast in the Baltic Sea and not higher than an altitude of 100 m. Therefore, more research is needed to improve the extrapolation of SAR wind speeds to hub height, and convince the industry to use them.

Machine learning seemed appropriate to us for improving SAR wind speeds retrieval due to the variety of error sources. We used a large network of metocean buoys to train the algorithm in order to cover a large range of sensor angles. Regarding the extrapolation to higher altitudes, machine learning also seemed appropriate to us due to the complexity of the problem. Machine learning has indeed been found to improve the accuracy of extrapolated wind speeds compared to power laws or logarithmic laws (Türkan et al., 2016; Mohandes and Rehman, 2018; Vassallo et al., 2019), and theoretical approaches (Optis et al., 2021). Moreoever, Bodini and Optis, 2020, have shown that a machine learning algorithm trained in one location can be applied in a large area around it without significantly degrading its performance. Another advantage of machine learning compared to theoretical approaches is that it is not limited to the boundary layer and can be trained at any altitude. As in Badger et al. (2016), we took advantage of a numerical model to assess the atmospheric stability and extract relevant meteorological parameters. These parameters were used as input to the machine learning algorithm, which was trained with Lidar wind profiles measured in the North Sea.

Section 2 describes the SAR data, the high-resolution numerical model, and the in-situ data used as a reference to train and validate the algorithms. Section 3 presents the algorithms and the method used to compute the extractible wind power. It also provides some insight about the effect of the number of samples on the method accuracy and a specific method for correcting SAR irregular temporal sampling. Section 4 presents the performance of the two machine learning algorithms and a test of the method in two areas off the Dutch coast. The resulting maps of the extractible wind resource are presented and compared with the outputs of the high-resolution numerical model in order to estimate the benefit of using this method compared with a state-of-the-art technique.

2 Data

2.1 Areas of study

The two areas of study are located off the Dutch coast (Figure 1). They have an approximate size of 70 x 70 km. Their geographic extent was defined in order to include offshore profiling Lidars and a part of the coastline in order to observe the wind speed coastal gradient.

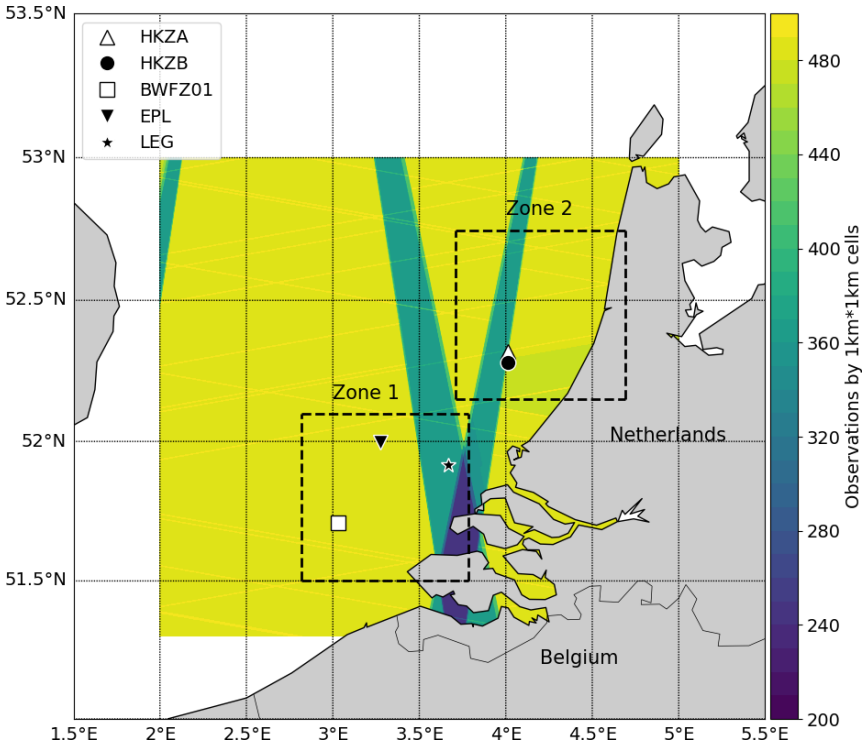

Figure 1: Locations of Zone 1 (bottom, latitude 51.50°N - 52.09°N / longitude 2.82°E - 3.77°E) and Zone 2 (top, latitude 52.15°N - 52.74°N / longitude 3.71°E - 4.68°E) with the positions of the profiling Lidars. The colour represents the number of Sentinel-1 SAR Level-2 observations during two years (June 2016 to June 2018).

2.2 Sentinel-1 SAR data

Sentinel-1 A and B are two polar-orbiting satellites equipped with C-band SAR. This sensor, which records surface roughness, has the advantage of operating day and night at wavelengths not impeded by cloud cover. Sentinel-1 Level-1 Ground Range Detected (GRD) backscatter product has a spatial resolution of a few tens of meters, whereas Level-2 wind products typically have a spatial resolution of 1 km. The two satellites are located on the same orbit 180° apart and at an altitude close to 700 km. In Dutch coastal waters, the acquisition mode is an Interferometric Wide swath using the TOPSAR

technique, which provides a better-quality product by enhancing the image homogeneity (De Zan and Guarnieri, 2006). The revisit rate is one passage every two days, which occurs around 5 AM or around 5 PM (UTC). The satellites pass in the morning or in the evening depending on the orbit orientation, descending or ascending, respectively. The exact acquisition time can vary by plus or minus 30 mn depending on the incidence angle under which the region of interest is observed. The number of samples over two years for the areas of interest is shown in Figure 1, on which it can be seen that the coverage is not spatially uniform.

The Level-1 images were calibrated and corrected from the instrument noise provided as metadata. A dedicated bright target filtering was applied to remove Radar echoes created by ships, wind farms and other structures at sea. An additional filter (Koch, 2004) was used to identify heterogeneous signatures not related to wind, like currents, Radar interferences, and remaining bright targets. However, this filter has an increased sensitivity at low wind speeds, therefore, the identified pixels were not removed to avoid disrupting the wind speed Weibull distribution, which is necessary to estimate wind power. The information provided by this filter was only used to create a quality flag indicating areas where wind power estimates are unreliable, typically due to dense regions of wind turbines or mooring areas (see Section 4). Then, Level-1 SAR products were degraded to a 1 km resolution and Level-2 surface winds at 10 m above sea level were created using a Bayesian inversion scheme using two inputs: the wind vector obtained by inverting SAR backscatter with the CMOD7 GMF (Stoffelen et al., 2017) and the wind vector obtained from the ECMWF Numerical Weather Prediction (NWP) model. Level-2 product tiles were finally combined into a gridded map over the areas of interest, in order to form a data cube where each pixel corresponds to a time series of SAR wind speed measurements.

2.3 High-resolution numerical model

We used the Weather Research and Forecasting (WRF) non-hydrostatic meso-scale model (Skamarock et al., 2019) with a resolution of 1 km. The Planetary Boundary Layer (PBL) parametrization of the model was based on Hahmann et al., 2020. The WRF was forced at its boundaries by a downscaled larger-scale model, the reanalyzed ERA5 (Hersbach etal., 2020) developed by ECMWF that has an hourly temporal resolution. The WRF was run over the areas of study from December 2015 to June 2018 in order to cover the period during which Lidar campaigns and Sentinel-1 data overlap.

The WRF provides wind speed and wind direction from sea level to 200 m with increments of 20 m, as well as other variables, such as air and sea surface temperature, surface heat flux, relative humidity, and pressure. These meteorological parameters were used to create the input parameters to the extrapolation algorithm. Moreover, since the WRF is typical of numerical models currently used by industry, we also used it as a reference to assess the benefits of using SAR data. Since the industry often combines numerical models with in-situ measurements, we also assessed the WRF outputs with the available Lidar data. The WRF was found to underestimate the extractible power by 3% on average over all Lidars. We corrected this bias before using the WRF as a reference in the maps presented in Section 4.

2.4 NDBC buoy network

The buoy dataset consists in 10-minutes averaged wind speeds from the National Data Buoy Center (NDBC) of the United States of America (USA). This network has the advantage of having a large number of instruments, a large spatial coverage, and a standardized processing and quality-check (Meindl & Hamilton, 1992). We selected only buoys measuring wind speed at 4 m, so that the dataset in homogeneous in height and obtained with a similar type of instrument. 12 buoys are located in the East coast of the USA (stations 41004, 41009, 41010, 41013, 41025, 41043, 44007, 44017, 44018, 44020, 44025, 44065), 18 in the West coast of the USA (stations 46011, 46012, 46014, 46015, 46022, 46025, 46026, 46027, 46028, 46041, 46042, 46047, 46050, 46053, 46054, 46069, 46084, 46086), 9 in the Golf of Mexico (stations 42002, 42003, 42012, 42035, 42036, 42039, 42055, 42056, 42060), and 3 around Hawaii islands (stations 51000, 51002, 51003).

2.5 Lidar data

The dataset comprises five ground-based profiling Lidars located off the Dutch coast (Figure 1). They are named HKZA, HKZB, BWFZ01, EPL and LEG. HKZ stand for Hollandse Kust Zuid wind farm, BWF for Borssele Wind Farm Zone, EPL for European Platform, and LEG for Lichteiland Goeree platform. Zone 1 includes Lidars BWFZ01, EPL and LEG, and Zone 2 includes Lidars HKZA and HKZB. Lidars HKZA, HKZB, BWFZ01 are floating, whereas Lidars EPL and LEG are installed on platforms. These Lidars provide 10-minutes averaged wind speeds and wind directions. The data were quality-checked by our data provider C2WIND (for each time intervals, the minimum number of packets was set at 20 and the minimum availability at 80%). The vertical sampling and the duration of these Lidar measurements vary between observation campaigns and are displayed in Table 1.

Lidar	Longitude	Latitude	First date	Last date	Number of levels	Lowest altitude	Highest altitude	SAR collocations
HKZA	4.011°E	52.309°N	2016-06-05	2018-06-05	11	30m	200m	327
HKZB	4.013°E	52.292°N	2016-06-05	2018-06-05	11	30m	200m	327
LEG	3.667°E	51.917°N	2014-11-17	2017-03-31	10	61m	300m	108
EPL	3.276°E	51.998°N	2016-05-30	2017-03-31	11	61m	290m	153
BWFZ01	3.033°E	51.71°N	2015-06-11	2017-02-27	10	30m	200m	188

Table 1: Main characteristics of the five profiling Lidars

Many of the Lidars altitude levels are similar to the ones of the WRF. However, when there was a difference, the Lidar wind speeds were extrapolated to the closest WRF level in order to obtain homogeneous measurements. Since the altitude differences were small, typically a few meters, this was done with a classical power law:

$$u_{\text{WRF level}} = u_{Lidar\ level} \cdot \left(\frac{z_{WRF\ level}}{z_{Lidar\ level}}\right)^{\alpha} \quad \text{Eq. (1)}$$

where z denotes the altitude in m, u the instantaneous wind speed in m s^{-1}, and α the non-dimensional power law exponent (set to 0.11, as recommended over sea by Hsu et al., 1994).

3 Methods

3.1 Correction of SAR surface wind speeds

Given the complex relation between sea state and wind speed, and the number of factors able to influence it, machine learning was found to be an appropriate technique to improve the accuracy of SAR surface winds. Since the wind speed error depends on the sensor geometry, the algorithm was trained with a large database of buoy measurements covering the diversity of possible angles. This database was obtained from the NDBC network of metocean buoys (see Section 2.4). As a result, the machine learning algorithm transforms SAR surface winds into equivalent 4 m standard buoy measurements. A total of 4419 collocated observations between NDBC buoys and Sentinel-1 SAR could be found.

We used a Gradient Boosting algorithm (Friedman, 2001), which is known to perform well in regression tasks. It was implemented with the XGBRegressor function of XGBoost Python package. Its architecture and hyper-parameters were chosen using grid-search with cross-validation. Regarding input parameters, we selected parameters having a link with SAR wind speed errors due to physics or to the retrieval algorithm specificities. Then, we plotted scatterplots of these parameters against SAR errors, and checked the correlation visually. The following parameters were finally selected: SAR wind speed (extrapolated to 4 m with Eq. (1)), SAR wind direction, difference between the azimuth angle (i.e., the angle between the North and the satellite track) and wind direction, incidence angle (i.e., the angle between the radar illumination and the zenith of the target), SAR backscatter, SAR cross-polarization backscatter (related to strong winds), instrument thermal noise, Unix time, and ECMWF wind speed provided as metadata (it improves low wind speeds accuracy). We also validated our choices a posteriori by estimating the relative importance of these parameters in the decision trees with the Shapely Additive Explanations (ShAP) method (Lundberg & Lee, 2017). The Gradient Boosting algorithm was trained with 80% of the data points randomly chosen, and the rest of them were used as a test dataset.

3.2 Extrapolation to hub height

In order to extrapolate SAR surface wind speeds to hub height, we first applied the correction algorithm described above to transform them into equivalent 4 m standard buoy measurements. This also removed their dependency on the sensor geometry, which was required since the extrapolation algorithm has to be trained with a small dataset of Lidars that do not cover all possible angles. Then, the extrapolation algorithm was trained with the Lidar dataset from the North Sea (Section 2.5) using as input corrected SAR surface wind speeds and meteorological parameters linked to the atmospheric stability extracted from the WRF (section 2.3). As a result, the algorithm does not require any in-situ instruments to function. Combining all measurement sites, more than 1000 collocated data-points between Lidars and Sentinel-1 SAR could be found. We transformed these data-points into triple collocations by adding the corresponding meteorological parameters extracted from the WRF.

Since the accuracy of numerical models is questionable, these meteorological parameters must be carefully chosen. In particular, the WRF wind speed at hub height could not be used directly because it would interfere with SAR estimates. Instead, we provided the algorithm with the WRF extrapolation ratio between the wind speed at the surface and hub height. However, when assessing the WRF against Lidars, we found that the WRF wind speed had an unrealistic bias below 40m. It was unclear if this was due to the PBL adapted to higher altitudes, to a lack of accuracy of the Lidars first levels, or to the power law extrapolating these first levels to a lower altitude. In any case, as a precaution, we used the extrapolation ratio between the WRF wind speed at 40 m and the WRF wind speed at hub height. This extrapolation ratio was found to be accurate: the comparison with experimental data showed that its bias was less than 1% for each Lidar. The other relevant parameters we selected were the air-sea temperature difference and the surface heat flux. The accuracy of these parameters is also problematic (see, i.e., Pena Diaz & Hahmann, 2012). However, in the context of machine learning, the focus is more on the information parameters contain, rather than on their absolute accuracy. Since they are not fluctuating as quickly as wind speed, we assumed that their biases were following repetitive patterns that could be learnt, and that these biases would not prevent the algorithm from extracting the relevant information. Here too, we used scatterplots to confirm the correlation between these parameters and the experimental extrapolation ratio, and checked their relative importance a posteriori with the ShAP method.

This second algorithm was also implemented with the XGBRegressor function of XGBoost Python package and its architecture was also chosen using grid-search with cross-validation. Since the final estimation of the extractible wind power has to be done Lidar per Lidar, and since its accuracy is very sensitive to the number of samples (see Section 3.4), we used a round-robin validation. This method consists in removing a Lidar from the dataset, training the algorithm with the remaining Lidars, assessing the performance with the Lidar that was not used, and then repeating the process with each Lidar. It allows the extractible wind power to be estimated with all the available samples for each Lidar. Another advantage of the round-robin validation is that the training is done in one location and the validation in another.

3.3 Extractible wind power estimation

The total wind power density is related to the cube of wind speed. Therefore, very high wind speeds have a strong influence on its estimation. Since SAR sensors do not detect them well because they saturate, we do not recommend using SAR data to estimate the total wind power density. However, SAR data can be used to estimate directly the extractible wind power, because wind turbines usually do not operate or function at a plateau when very high wind speeds occur. The extractible wind power, denoted P in the following, is obtained by multiplying point-by-point the wind speed probability density function (pdf) by the power curve of a wind turbine. In this study, we chose to simulate a typical 10MW turbine operating at 119m: the DTU 10 MW Reference Wind Turbine V1 (DTU Wind Energy, 2017). Its power curve is available at https://github.com/NREL/turbine-models/blob/master/Offshore/DTU_10MW_178_RWT_v1.csv, last accessed September 2, 2021. A simple histogram could be used to estimate the wind speed pdf. However, due to the limited number of SAR samples, a more efficient technique consists in fitting SAR data with a Weibull pdf, which usually describes wind speed accurately. The Weibull pdf is:

$$pdf(u) = \frac{k}{\lambda}\left(\frac{u}{\lambda}\right)^{k-1} e^{-(u/\lambda)^k} \quad \text{Eq. (2)}$$

where λ is a scale parameter in m s^{-1} and k a dimensionless shape parameter. These parameters can be obtained by using the method of the moments with the following formulas (Pavia and O'Brien, 1986):

$$k = (\sigma/\mu)^{-1.086} \quad \text{Eq. (3)}$$

$$\lambda = \frac{\mu}{\Gamma\left(\frac{1}{k}+1\right)} \quad \text{Eq. (4)}$$

where μ is the mean wind speed, σ the wind speed standard deviation, both in m s^{-1}, and Γ the Gamma function. Since the mean wind speed and its standard deviation are directly linked to the wind speed pdf, an accurate estimation of these first two moments is enough to obtain the extractible power and achieve a low error.

3.4 Effect of the number of samples on the accuracy

The accuracy of this estimation method was assessed with simulations by generating time-series of a Weibull random variable with arbitrary parameters, and then trying to recover the original parameters from these time-series. More specifically, we chose Weibull parameters typical of the North Sea wind climate (k = 2.2 and λ = 8.5) and computed the reference extractible power using the exact formula (Eq. (2) multiplied point-by-point by the 10 MW turbine power curve).

Then, we generated random synthetic wind speed time-series using the Weibull pdf (Eq. (2)) with these parameters and applied the method of the moment (Eq. (3) and Eq. (4)) to estimate these original parameters and the extractible power. Figure 2 shows the extractible power error as a function of the number of samples in the synthetic time-series. With 500 samples, which is approximately the number of SAR samples used in this study, the accuracy is ± 3%. Note that, in industrial applications, we expect a higher accuracy since other satellites (like Envisat and Radarsat) would be used together with Sentinel-1 to cover a period of more than twenty years, thus providing a number of samples comprised between 1000 and 1500.

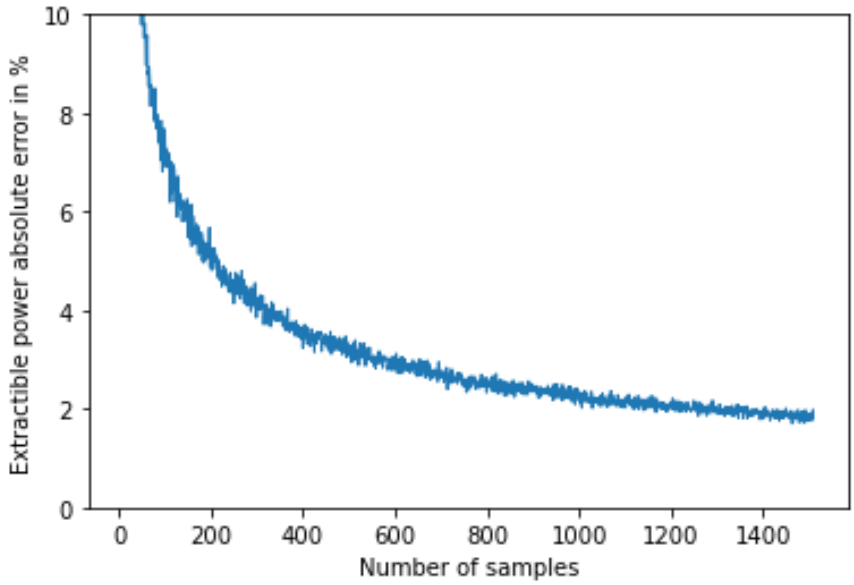

Figure2: Accuracy of the method of the moment for estimating the extractible wind power as a function of the number of sample.

3.3 Correction of SAR low temporal sampling

The main limitation of SAR satellites is their low temporal sampling (one passage every two days for Sentinel-1 in Europe). This limitation actually guarantees the statistical independence of measurements. Nevertheless, since SAR satellites are on a sun-synchronous orbit, they pass always at the same times of the day, in the morning or in the evening. As a result, they cannot fully see the intraday variability of wind speed. Moreover, the monthly and yearly sampling can also be irregular due to space missions' start and end dates and operational constraints.

However, the intraday variability of wind speed is low (Van der Hoven, 1957) and close to a 24 h period sinusoid (Figure 3). Therefore, since Sentinel-1 satellites pass at two possible times of the day separated by 12 h, according to the Nyquist-Shannon sampling theorem, they should still be able to capture the intraday variability. In order to verify this, we computed the mean wind speed and the extractible wind power using only Lidar measurements at 5 AM and 5 PM (UTC). Then, we compared these results to the ones obtained using all Lidar measurements at any time of day. For all Lidar, the differences were found to be below 0.5% and 1%, respectively (Table 2). Therefore, SAR satellites are indeed able to capture most of the wind intraday variability. However, this conclusion might not be true in geographical areas where thermic winds are stronger than in the North Sea.

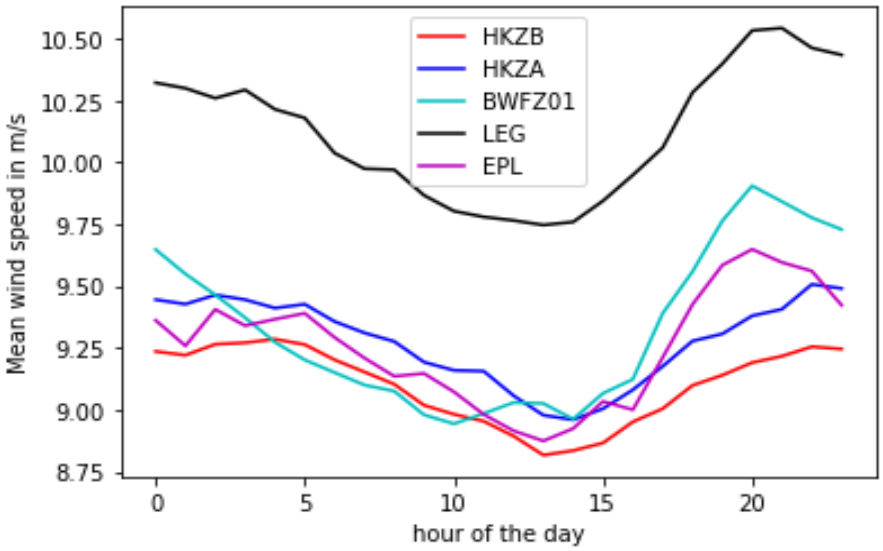

Figure 3: Intraday variability of the mean wind speed at 120 m for each Lidar. The time is given in UTC, which is close to the local time since Zone 1 and Zone 2 are located near Greenwich meridian (LEG curve is higher because the campaign was performed during winter).

Lidar	Error of the mean wind speed in %	Error of the extractible wind power error in %
HKZA	-0.34	-0.16
HKZB	-0.23	-0.01
LEG	0.36	0.94

EPL	-0.04	0.06
BWFZ01	-0.47	-0.08

Table 2: Estimation of the errors of the mean wind speed and the extractible wind power due to SAR low temporal sampling.

Although the effect of the intraday variability is expected to be low, in order to improve the accuracy of our method, we decided to correct the errors related to SAR low and irregular sampling. These errors were removed by simulating exactly all the satellites' passages over the WRF outputs: for each pixel of the areas of study, we computed the mean wind speed produced by the WRF and compared it to the mean wind speed seen by the satellites. The difference was used to correct SAR mean wind speed.

4 Results

4.1 Performance against buoys at 4 m

The correction algorithm hyper-parameters optimized with grid-search are shown in Table 3 (left column). The other hyper-parameters are the default ones. The relative importance of the input parameters is given in Figure 4. As expected, the parameters related to geometry and to low and high wind speeds contain the most useful information. The algorithm was able to reduce the bias of SAR wind speed estimated at 4 m above sea level from -0.48 m s^{-1} to 0.02 m s^{-1}, its mean absolute error (MAE) from 0.85 m s^{-1} to 0.57 m s^{-1}, and it standard deviation from 0.95 m s^{-1} to 0.74 m s^{-1}. Figures 5 shows the scatterplots of SAR wind speeds against buoys before and after applying machine learning. The bias is indeed reduced and the cloud of points is thinner after machine learning.

Hyper-parameter	**Correction of surface winds**	**Extrapolation to hub height**
objective	Squared error	Squared error
learning rate	0.03	0.03
max_depth	5	6
min_child_weight	0	0

min_split_loss	0.02	0.02
subsample	0.99	0.99
colsample_bytree	1	1
reg_alpha	0.5	0.
reg_beta	0.8	0.7
n_estimators	320	350

Table 3: Gradient Boosting hyper-parameters optimized with grid-search with cross-validation.

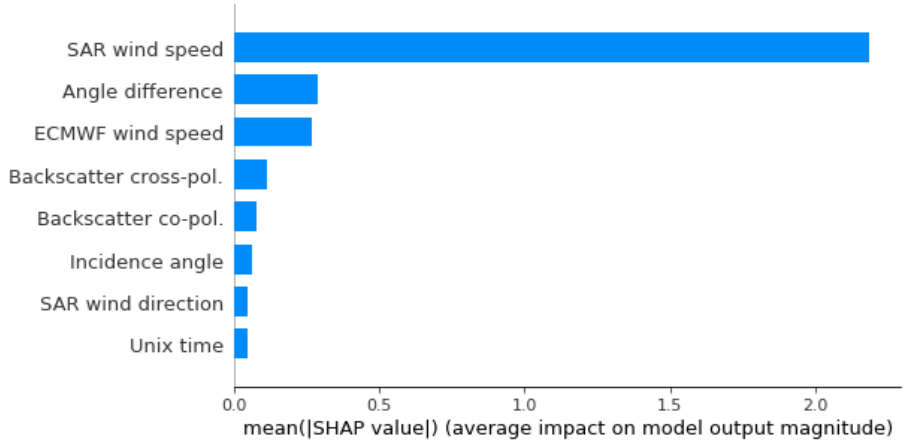

320

Figure 4: Relative importance of the input parameters used to correct the SAR surface winds.

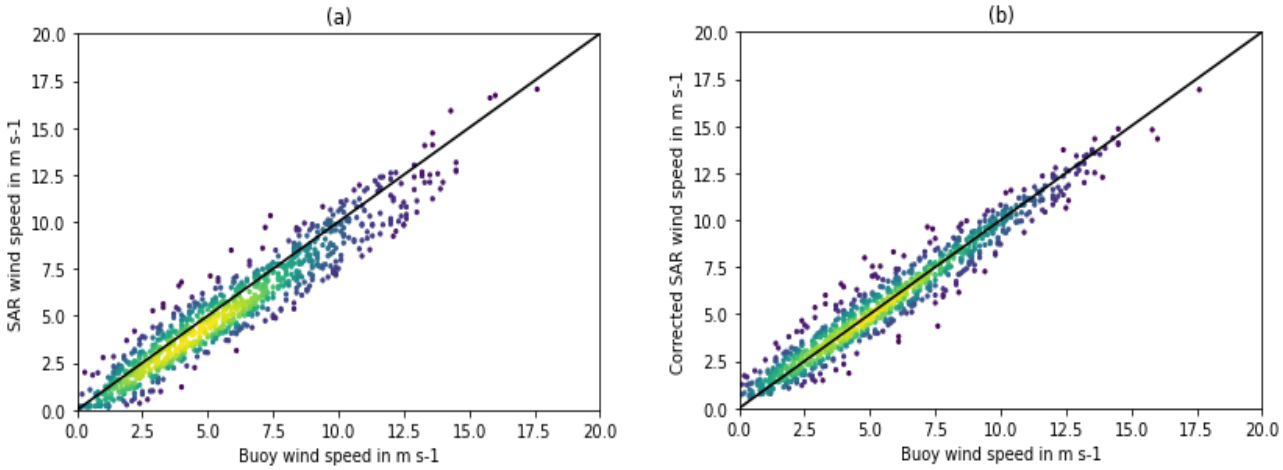

325

Figure 5: Scatterplots between SAR and buoy wind speeds at 4 m above sea level before machine learning (a) and after machine learning (b) using the test dataset. The colours represent the density of points and the black curve is the identity line.

330 **4.2 Performance against Lidars**

The extrapolation algorithm hyper-parameters optimized with grid-search are shown in Table 3 (right column). The relative importance of the input parameters is given in Figure 6. It can be seen that the surface net heat flux is the most relevant atmospheric stability parameter. The algorithm performance against Lidars is shown in Figure 7 for various altitudes up to 200 m. At 120 m, which is the hub height of the simulated turbine, the bias of SAR wind speed is 0.16 m s^{-1}, its MAE 0.99 m
335 s^{-1} and its standard deviation 1.43 m s^{-1}. We also extrapolated corrected SAR wind speeds to higher altitudes assuming the power law given by Eq. (1) for comparison. Figures 8 shows the scatterplots against Lidars of SAR wind speeds extrapolated with the power law and with machine learning. It can be seen that the dispersion is reduced significantly with machine learning. Figure 9 shows the final biases of SAR mean wind speed and SAR extractible power against each Lidar at various altitudes. These biases remain comprised within ± 3% up to 200 m. As explained previously, an even higher accuracy is
340 expected in a real industrial application, because the number of samples used here is limited by the short duration of the Lidar campaigns used as a reference.

These results need to be confirmed in other geographical locations than the North Sea. Nevertheless, in a region having a very different wind pattern and no Lidar measurement available, a simpler method can be applied. The extrapolation ratio provided by the high-resolution numerical model can be used directly to extrapolate SAR surface winds without applying
345 machine learning. In that case, the extractible wind power error was found to be comprised within ± 7%, which is still accurate enough to provide some insight compared to a numerical model alone.

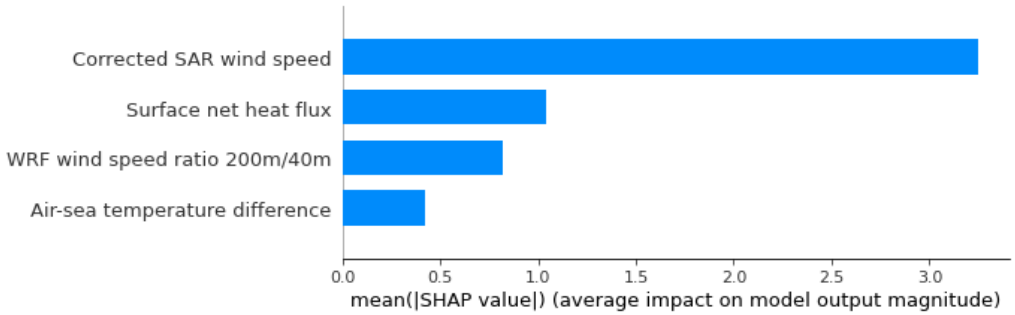

Figure 6: Relative importance of the input parameters used to extrapolate SAR surface winds to higher altitudes.

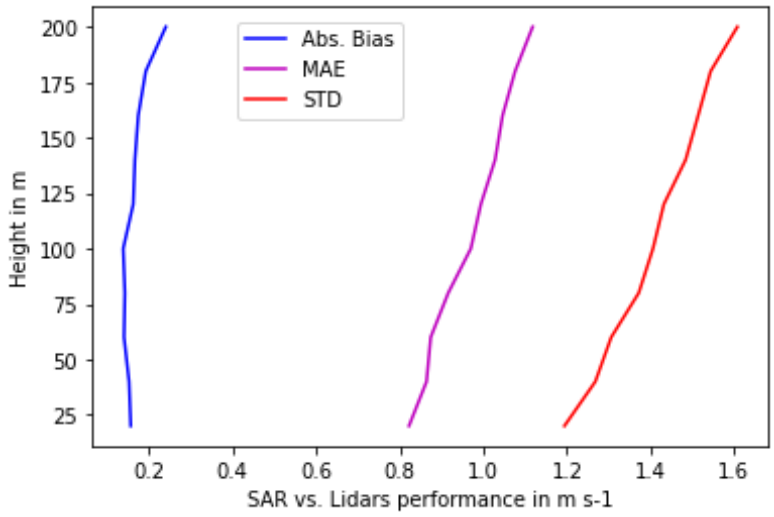

Figure 7: Performance of the machine learning algorithm extrapolating corrected SAR surface winds to higher altitudes.

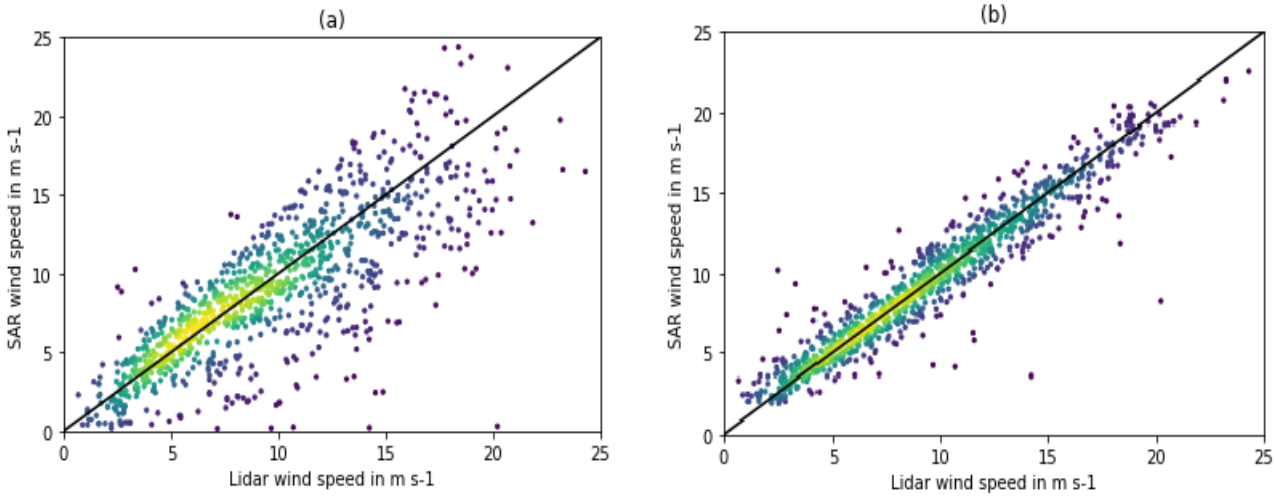

Figure 8: Scatterplots between SAR and Lidar wind speeds at 120 m above sea level when the extrapolation is performed with a classical power law (a) or with machine learning (b). The colours represent the density of points and the black curve is the identity line.

365

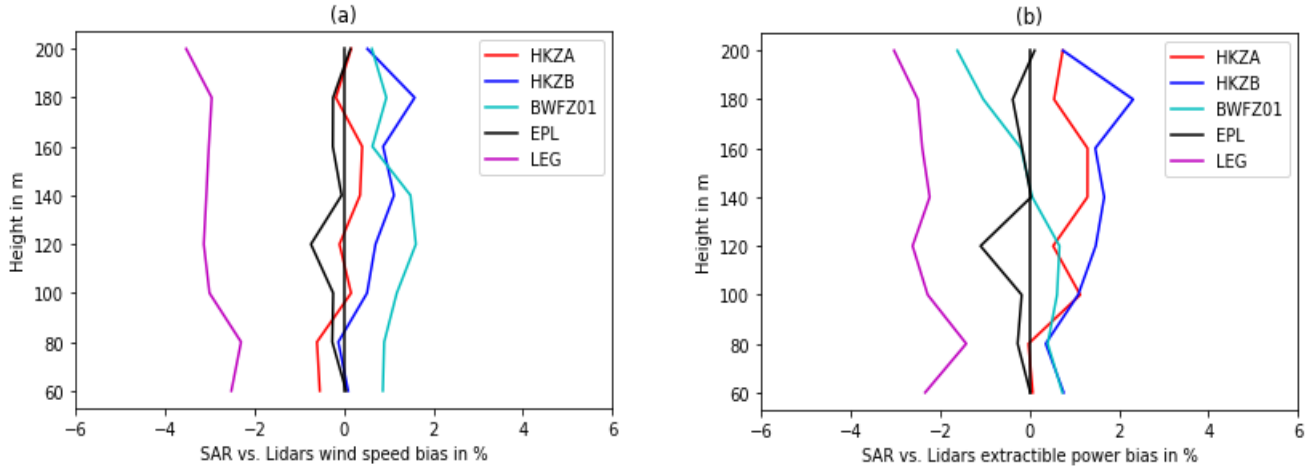

Figure 9: Biases of SAR extrapolated wind speed (a) and extractible wind power (b) against each Lidar in percentage. The results with Lidar LEG are less accurate due to its low number of collocated SAR samples.

370

4.3 Wind power maps at hub height

Figures 10 and 11 show the extractible wind power produced at 120 m over the areas of study by the WRF and SAR satellites, and the difference between them in percentage. It can be seen that the use of SAR data significantly increases the level of detail compared to WRF outputs. In particular, the coastal wind speed gradient, which is often crucial in offshore site assessment, is resolved by the SAR and not by the WRF (see the gradients on Figure 12). Therefore, SAR data can be used to optimize the required distance from the coast and minimize wind farm projects risks.

Some artefacts are still visible on the maps and need to be corrected in the future. As explained in Section 2.2, the presence of these artefacts was measured by a Koch filter and a quality flag was created. Figures 10 and 11 also show the percentage of SAR data flagged as 'low quality'. These areas are mainly due to bright targets that could not be filtered related to existing wind farms having a high density of turbines and areas where a large numbers of stationary shipping vessels are anchored. In addition, in Zone 1, unrealistic waves can be seen close to the coast. These patterns correspond to similar waves of sand in the seabed. The bathymetry in these shallow waters seems to affect currents and, therefore, the SAR backscatter. Regarding swath edges that can still be seen, the problem arises from a difficulty in estimating the wind speed standard deviation when the number of sample is low. We expect this problem to disappear if more SAR samples are used. In an industrial application, the total number of SAR samples would be comprised between 1000 an 1500, instead of less than 300 here in the worst case.

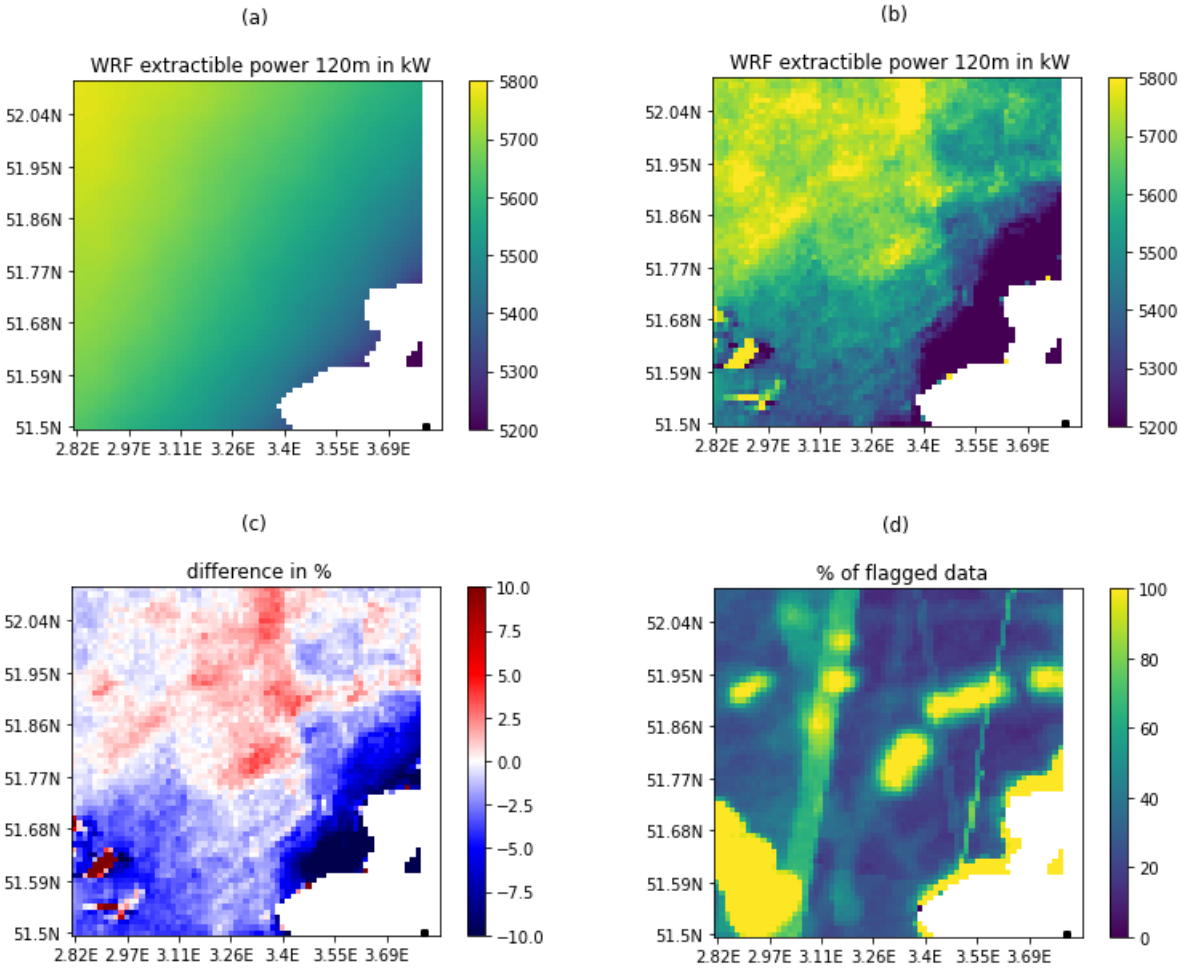

390

Figure 10: Wind resource at 120 m over Zone 1 assuming a typical 10 MW turbine: extractible wind power in kW predicted by the WRF (a) and SAR satellites (b), difference in percentage (c), and percentage of low quality SAR data (d).

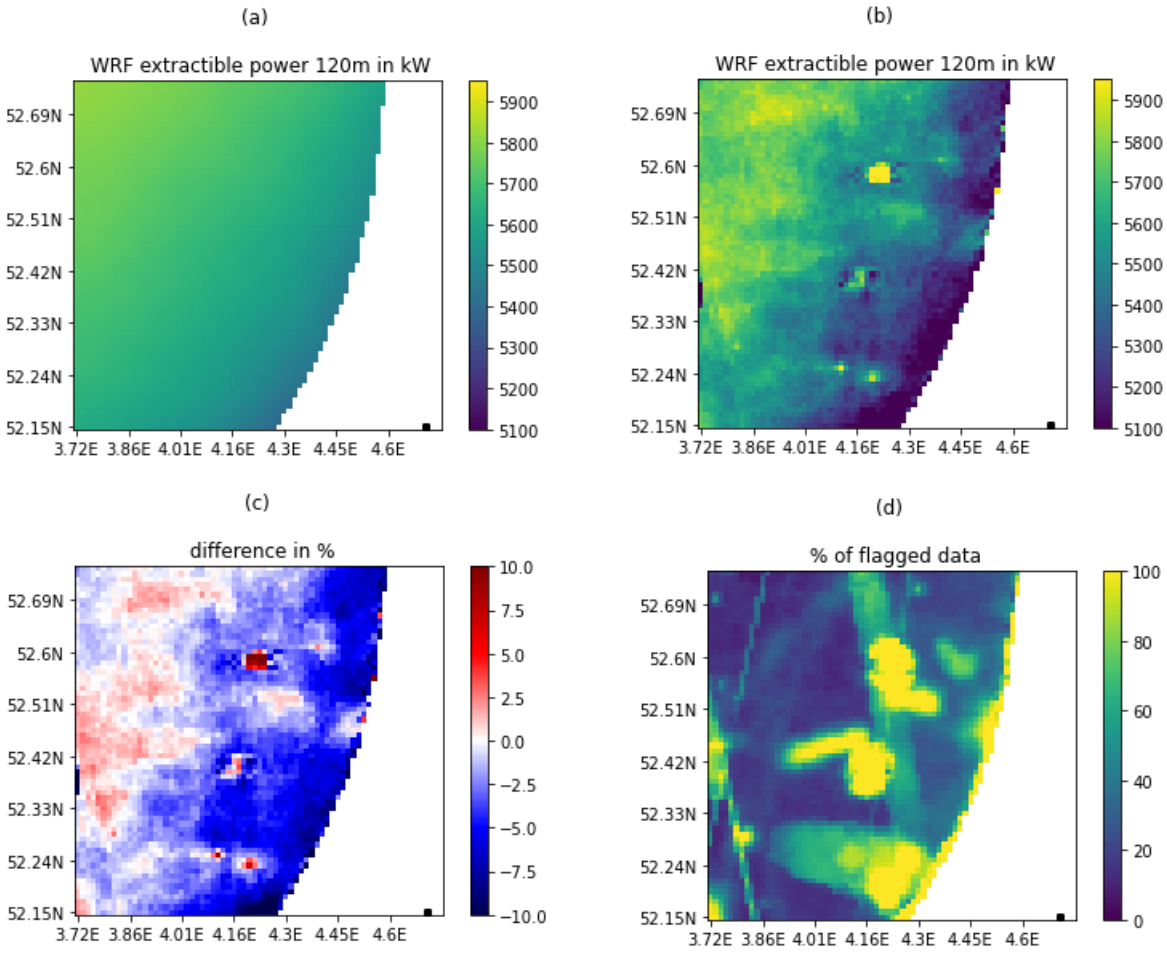

395 **Figure 11: Wind resource at 120 m over Zone 2 assuming a typical 10 MW turbine: extractible wind power in kW predicted by the WRF (a) and SAR satellites (b), difference in percentage (c), and percentage of low quality SAR data (d).**

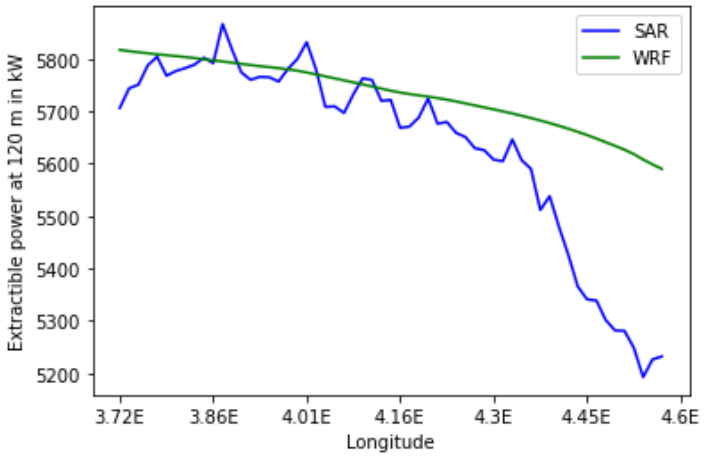

Figure 12: Extractible wind power coastal gradient at 120 m on a horizontal line at the top of Zone 2 estimated by the WRF and by SAR satellites.

5 Conclusion

A new method for estimating offshore wind resource at hub height using SAR and machine learning has been presented. The method has three main steps. Firstly, SAR Level-1 products are homogeneously reprocessed into Level-2 surface winds products. These wind speeds are corrected with a machine learning algorithm using geometrical parameters of the SAR sensor and SAR metadata to compensate for systematic errors attributed to the GMF or SAR calibration. This algorithm is trained with a large network of metocean buoys. Secondly, SAR surface winds are extrapolated to higher altitudes with another machine learning algorithm using meteorological parameters extracted from a high-resolution numerical model. This algorithm is trained with a dataset of Lidar vertical wind profiles. Then, thirdly, the wind speed Weibull parameters are estimated taking into account SAR irregular sampling. Finally, a wind turbine is simulated and the extractible wind power is computed by multiplying point-by-point the wind speed pdf by its power curve.

This first machine learning algorithm correcting SAR surface wind speeds was tested against 4 m high buoy measurements. The resulting SAR wind speed bias is 0.02 m s^{-1}. Its MAE is 0.57 m s^{-1} and its standard deviation 0.74 m s^{-1}. This algorithm can be used as a standalone to improve the accuracy of SAR wind products. The second algorithm extrapolating surface winds to higher altitudes has been tested against Lidar measurements up to 200 m. At 120 m, which is the hub height of the simulated turbine, the extrapolated wind speed bias is 0.16 m s^{-1}. Its MAE is 0.99 m s^{-1} and its standard deviation 1.43 m s^{-1}.

This algorithm can also be used as a standalone to extrapolate wind speeds measured at 4 m above sea level. These two algorithms combined together produce instantaneous SAR wind fields at hub height, which can provide interesting insights to wind farm developers. When these SAR wind speeds at hub height are converted into a potential extractible wind power, at 120 m, the accuracy was 3% against Lidars. Since this assessment was done with a low number of SAR samples due to the limited duration of Lidar campaigns, a higher accuracy is expected in an industrial application.

The method was tested in two areas off the Dutch coast. Compared to the maps provided by the WRF numerical model, this method has the advantage of providing a much higher level of details thanks to the 1 km resolution provided by SAR surface wind measurements. The most striking result is that wind resource maps based on SAR are able to resolve the wind speed coastal gradient. Therefore, using SAR data combined with machine learning can improve the accuracy of offshore wind resource estimates at hub height and provide useful insights to optimize wind farm siting and risk management.

Further research should focus on removing remaining artefacts on the SAR maps, such as swath edges, bright targets, and the effect of bathymetry. Moreover, since the method was validated using Lidars only located in the North Sea, the extrapolation algorithm may not be adapted to meteorological conditions in seas having a different wind climate. In that case, wind profiles measured by Lidars located in the region of interest would need to be included in the training dataset and used to validate the method again.

Code and data availability

Level-1 SAR data are available on ESA scihub website. Buoys data are available at NDBC. Lidar data are available at the Dutch Ministry of Economic Affairs and Climate Policy. The WRF source code and Python packages are open source. Unfortunately, the full code of the method developed in this paper is not available due to corporate constraints.

Authors' contribution

Louis de Montera designed the algorithm and wrote the paper, Henrick Berger processed the SAR raw data and created a Level-2 gridded wind product. Romain Husson provided his expertise on SAR satellite and wind measurement from space. Pascal Appelghem parametrized the WRF model and performed the runs. Laurent Guerlou and Mauricio Fragoso supervised the study, organised the funding, and gathered together the project team.

Competing interests

The authors declare that they have no conflict of interest.

Acknowledgments

We would also like to thank Rémi Gandoin from C2WIND for checking the quality of the Lidar data, Cynthia Johnson for correcting the spelling and improving the article style, and three anonymous referees for their contributions.

Financial support

This research was funded by the French Space Agency (Centre National d'Etudes Spatiales).

References

Ahsbahs, T., Badger, M., Karagali, I. and Guo Larsén, X.: Validation of Sentinel-1A SAR coastal wind speeds against scanning LiDAR. Remote sensing, 9(6), doi: 10.3390/rs906055, 2017.

Ahsbahs, T., MacLaurin, G., Draxl, C., Jackson, C., Monaldo, F. and Badger, M.: US East Coast synthetic aperture radar wind atlas for offshore wind energy. Wind Energy Science, 5, 1191-1210. doi: 10.5194/wes-5-1191-2020, 2020.

Badger, M., Peña, A., Hahmann, A. N., Mouche, A. A. and Hasager, C. B.: Extrapolating Satellite Winds to Turbine Operating Heights, J. Applied Meteorology and Climatology, 55(4), 975-991, doi: 10.1175/JAMC-D-15-0197.1, 2016.

Badger, M., Ahsbahs, T. T., Maule, P. and Karagali, I.: Inter-calibration of SAR data series for offshore wind resource assessment. Remote Sensing of Environment, 232, 111316, doi: 10.1016/j.rse.2019.111316, 2019.

Bentamy, A. and Croize-Fillon, D.: Spatial and temporal characteristics of wind and wind power off the coasts of Brittany. Renewable energy, 66, 670-679, doi: 10.1016/j.renene.2014.01.012, 2014.

Breiman, L.: Random Forests, Machine Learning, 45(1), 5-32, 2001, doi: 10.1023/A:1010933404324

Bodini, N. and Optis, M.: The importance of round-robin validation when assessing machine-learning-based vertical extrapolation of wind speeds. Wind Energy Science, 5(2), 489–501, doi:10.5194/wes-5-489-2020, 2020.

Chang, R., Zhu, R., Badger, M., Hasager, C.B., Zhou, R., Ye, D. and Zhang, X.: Applicability of synthetic aperture radar wind retrievals on offshore wind resources assessment in Hangzhou bay, China. Energies, 7, 3339-3354. doi: 10.3390/en7053339, 2014.

Chang, R., Zhu, R., Badger, M., Hasager, C.B., Xing, X. and Jiang, Y.: Offshore wind resources assessment from multiple satellite data and WRF modeling over South China sea. Remote Sensing, 7, 467-487, doi: 10.3390/rs70100467, 2015.

Christiansen, M. B., Koch, W., Horstmann, J., Hasager, C. B. and Nielsen, M.: Wind resource assessment from C-band SAR. Remote Sensing of Environment, 105, 68-81, doi: 10.1016/j.rse.2006.06.005, 2006.

De Zan, F. and Guarnieri, A. M.: TOPSAR: Terrain Observation by Progressive Scans. IEEE Trans. on Geoscience and Remote Sensing, 44(9), 2352-2360, doi: 10.1109/TGRS.2006.873853, 2006.

Pena Diaz, A., & Hahmann, A. N.: Atmospheric stability and turbulence fluxes at Horns Rev — an intercomparison of sonic, bulk and WRF model data. Wind Energy, 15(5), 717–731, https://doi.org/10.1002/we.500, 2012.

DTU Wind Energy. HAWC2 Model for the DTU 10-MW Reference Wind Turbine. 2017. https://www.hawc2.dk/Download/HAWC2-Model/DTU-10-MW-Reference-Wind-Turbine, last accessed September 2, 2021.

Friedman, J. H.: Greedy function approximation: A gradient boosting machine. Ann. Statist., 29(5), pp. 1189 - 1232, https://doi.org/10.1214/aos/1013203451, 2001.

Grachev, A. A. and Fairall, C. W.: Dependence of the Monin-Obukhov stability parameter on the bulk Richardson number over the ocean, J. Applied Meteorology, 36, 406–414, doi: 10.1175/1520-0450(1997)036<0406:DOTMOS>2.0.CO;2, 1996.

Hahmann, A. N., Sīle, T., Witha, B., Davis, N. N., Dörenkämper, M., Ezber, Y., García-Bustamante, E., González-Rouco, J. F., Navarro, J., Olsen, B. T., & Söderberg, S.: The making of the New European Wind Atlas – Part 1: Model sensitivity. Geoscientific Model Development, 13(10), 5053-5078, doi: 10.5194/gmd-13-5053-2020, 2020.

Hasager, C.B., Frank, H.P. and Furevik, B.R.: On offshore wind energy mapping using satellite SAR. Canadian Journal of Remote Sensing, 28(1), 80-89, doi: 10.5589/m02-008, 2002.

Hasager, C.B., Nielsen, M., Astrup, P., Barthelmie, R., Dellwik, E., Jensen, N.O., Jørgensen, B.H., Pryor, S.C., Rathmann, O. and Furevik, B.R.: Offshore wind resource estimation from satellite SAR wind field maps. Wind energy, 8, 403-419, doi: 10.1002/we.150, 2005.

Hasager, C.B., Barthelmie, R.J., Christiansen, M.B., Nielsen, M. and Pryor, S.C.: Quantifying offshore wind resources from satellite wind maps: study area the North Sea. Wind energy, 9, 63-74. doi: 10.1002/we.190, 2006.

Hasager, C.B., Badger, M., Peña, A., Larsén, X.G. and Bingöl, F.: SAR-Based Wind Resource Statistics in the Baltic Sea. Remote Sensing, 3, 117-144, doi: 10.3390/rs3010117, 2011.

Hasager, C. B., Mouche, A., Badger, M., Bingöl, F., Karagali, I., Driesenaar, T., Stoffelen, A., Peña, A. and Longépé, N.: Offshore wind climatology based on synergetic use of Envisat ASAR, ASCAT and QuikSCAT. Remote sensing of environment, 156, 247–263, doi: 10.1016/j.rse.2014.09.030, 2015.

Hasager, C.B., Hahmann, A.N., Ahsbahs, T., Karagali, I., Sile, T., Badger, M. and Mann, J.: Europe's offshore winds assessed with synthetic aperture radar, ASCAT and WRF, Wind Energy Science, 5(1), 375-390, doi: 10.5194/wes-5-375-2020, 2020.

Hersbach, H., Bell, B., Berrisford, P., Hirahara, S., Horányi, A., Muñoz□Sabater, J., Nicolas, J., Peubey, C., Radu, R., Schepers, D., Simmons, A., Soci, C., Abdalla, S., Abellan, X., Balsamo, G., Bechtold, P., Biavati, G., Bidlot, J., Bonavita, M., Chiara, G.D., Dahlgren, P., Dee, D., Diamantakis, M., Dragani, R., Flemming, J., Forbes, R.G., Fuentes, M., Geer, A.J., Haimberger, L., Healy, S.B., Hogan, R.J., Holm, E.V., Janisková, M., Keeley, S.P., Laloyaux, P., Lopez, P., Lupu, C., Radnoti, G., Rosnay, P.D., Rozum, I., Vamborg, F., Villaume, S., & Thepaut, J.: The ERA5 global reanalysis. Quarterly Journal of the Royal Meteorological Society, 146, 1999-2049, doi:10.1002/qj.3803, 2020.

Hsu, S. A., Meindl, E. A. and Gilhousen, D. B.: Determining the power-law wind-profile exponent under near-neutral stability conditions at Sea, Journal of Applied Meteorology and Climatology, 33(6), 757-765, doi: 10.1175/1520-0450(1994)033<0757:DTPLWP>2.0.CO;2, 1994.

Karagali, I., Peña, A., Badger, M. and Hasager, C. B.: Wind characteristics in the North and Baltic Seas from the QuikSCAT satellite. Wind energy, 17(1), 123-140. doi:10.1002/we.1565, 2014.

Koch, W.: Directional Analysis of SAR Images Aiming at Wind Direction. IEEE Transactions on Geoscience and Remote Sensing, 42(4), 702–710, doi: 10.1109/TGRS.2003.818811, 2004.

Lundberg, S., and Lee, S.: A unified approach to interpreting model predictions. Advances in Neural Information Processing Systems 30, 2017.

Meindl, E. A., and Hamilton, G. D.: Programs of the National Data Buoy Center. Bulletin of the American Meteorological Society, 73(7), pp. 985-994, https://doi.org/10.1175, 1992.

Mohandes, M. A. and Rehman, S.: Wind speed extrapolation using machine learning methods and LiDAR measurements. IEEE Access, 6, 77634-77642, doi: 10.1109/ACCESS.2018.2883677, 2018.

de Montera, L., Remmers, T., O'Connell, R. and Desmond, C.: Validation of Sentinel-1 offshore winds and average wind power estimation around Ireland, Wind Energy Science, 5(3), 1023-1036, doi: 10.5194/wes-5-1023-2020, 2020.

NREL. Best Practices for the Validation of U.S. Offshore Wind Resource Models. Optis, M., Bodini, N., Debnath, M., and Doubrawa, P., 2020, https://www.nrel.gov/docs/fy21osti/78375.pdf, last accessed 24 August 2021.

Optis, M., Bodini, N., Debnath, M., and Doubrawa, P.: New methods to improve the vertical extrapolation of near-surface offshore wind speeds, Wind Energ. Sci. Discuss. [preprint], doi: 10.5194/wes-2021-5, in review, 2021.

Pavia, E. G. and O'Brien, J. J.: Weibull Statistics of Wind Speed over the Ocean. Proceedings of the Royal Society of Mathematical, Physical and Engineering Sciences., 25(10), 1324-1332, doi: 10.1175/1520-0450(1986)025<1324:WSOWSO>2.0.CO;2 , 1986.

Pimenta, F., Kempton, W. and Garvine, R.: Combining meteorological stations and satellite data to evaluate the offshore wind power resource of Southeastern Brazil. Renewable energy, 33(11), 2375-2387, doi: 10.1016/j.renene.2008.01.012, 2008.

Remmers, T., Cawkwell, F., Desmond, C., Murphy, J., and Politi, E.: The Potential of Advanced Scatterometer (ASCAT) 12.5 km Coastal Observations for Offshore Wind Farm Site Selection in Irish Waters. Energies, 12(2), 206, doi: 10.3390/en12020206, 2019.

Sánchez, R. F., Relvas, P., and Pires, H. O.: Comparisons of ocean scatterometer and anemometer winds off the southwestern Iberian Peninsula. Continental shelf research, 27(2), 155-175, doi: 10.1016/j.csr.2006.09.007, 2007.

Skamarock, W. C., J. B. Klemp, J. Dudhia, D. O. Gill, Z. Liu, J. Berner, W. Wang, J. G. Powers, M. G. Duda, D. M. Barker, and X.-Y. Huang: A Description of the Advanced Research WRF Version 4. NCAR Tech. Note NCAR/TN-556+STR, 145 pp., doi:10.5065/1dfh-6p97, 2019.

Stoffelen, A., Verspeek, J. A., Vogelzang, J., and Verhoef, A.: The CMOD7 Geophysical Model Function for ASCAT and ERS Wind Retrievals. IEEE Journal of Selected Topics in Applied Earth Observations and Remote Sensing, 10(5), pp. 2123-2134, doi: 10.1109/JSTARS.2017.2681806, 2017.

Tieo, J.-., Skote, M., and Narasimalu, S:. Suitability of power-law extrapolation for wind speed estimation on a tropical island. Journal of Wind Engineering and Industrial Aerodynamics. 205, 104317, doi: 10.1016/j.jweia.2020.104317, 2020.

Türkan, Y. S., Yumurtacı Aydoğmuş, H. and Erdal, H.: The prediction of the wind speed at different heights by machine learning methods. Inter. J. of Optimization and Control: Theories & Applications, 6(2), 179–187. doi: 10.11121/ijocta.01.2016.00315, 2016.

Vassallo, D., Raghavendra K., and Harindra J. S. F.: Decreasing wind speed extrapolation error via domain-specific feature extraction and selection. Wind Energy Science, 5(3), doi: 10.5194/wes-5-959-2020, 2020.

Van der Hoven, I.: Power spectrum *of* horizontal wind speed *in the* frequency range *from* 0.0007 *to* 900 cycles per hour. J. Meteorol., 14(2), pp. 160–164, https://doi.org/10.1175/1520-0469(1957)014<0160:PSOHWS>2.0.CO;2>, 1957.